Deceleration of one-dimensional mixing by discontinuous mappings

Hannah Kreczak*
EPSRC CDT in Fluid Dynamics, University of Leeds, Leeds LS2 9JT, United Kingdom

Rob Sturman
School of Mathematics, University of Leeds, Leeds LS2 9JT, United Kingdom

Mark C. T. Wilson
School of Mechanical Engineering, University of Leeds, Leeds LS2 9JT, United Kingdom
(Received 17 August 2017; published 27 November 2017)

We present a computational study of a simple one-dimensional map with dynamics composed of stretching, permutations of equally sized cells, and diffusion. We observe that the combination of the aforementioned dynamics results in eigenmodes with long-time exponential decay rates. The decay rate of the eigenmodes is shown to be dependent on the choice of permutation and changes nonmonotonically with the diffusion coefficient for many of the permutations. The global mixing rate of the map M in the limit of vanishing diffusivity approximates well the decay rates of the eigenmodes for small diffusivity, however this global mixing rate does not bound the rates for all values of the diffusion coefficient. This counterintuitively predicts a deceleration in the asymptotic mixing rate with an increasing diffusivity rate. The implications of the results on finite time mixing are discussed.

DOI: 10.1103/PhysRevE.96.053112

I. INTRODUCTION

Mixing processes occur in a variety of industrial and natural applications with large variations in time and length scales, however the outcomes of mixing are typically the same; there is a reduction of length scales, an increase in the material interface, and an approach to uniformity. Good mixing can be accomplished in fluids by the action of stretching and folding (SF) fluid elements either through a cascade to small scales via turbulent eddies or stirring protocols which consider chaotic trajectories in highly viscous fluids [1]. The kinematic behavior of SF systems is captured well by the language of dynamical systems [2]. However, cutting and shuffling (CS), another mixing process, can increase the number of interfaces and can increase segregation but does not involve material deformation. Discontinuous transformations, such as cutting and shuffling, have more subtle dynamics and are not well understood. Once there is a reduction in length scales by an advective process, molecular diffusion will blur any large gradients achieving uniformity of a scalar field in the long-time limit.

There are many instances in mechanical mixing in which discontinuities arise, although there is comparatively little understanding in their implication on mixing. Split-and-recombine micromixers adopt the action of cutting and shuffling to increase the number of lamellae between substances [3]. Sink-source flows, which may be configured to generate chaotic velocity profiles via pressure differences from fluid subtraction and reinjection, can introduce discontinuities by the closing and opening of valves during syringe reorientation [4,5]. Streamline jumping, which occurs during reorientation, has been known to destroy dynamical features [6] or in the cut-dominated limit create pseudoelliptic and pseudohyperbolic periodic points [7]. Additionally, underlying properties of the material may introduce discontinuities. High strain in polymeric, plastic, or metallic materials may cause slip deformations due to shear banding [8]. Granular materials also exhibit the mechanisms of both stretching and folding and cutting and shuffling. In tumbler flows, a flowing layer at the surface introduces shearlike behavior while the bulk material undergoes solid body rotation. Piecewise isometries have been shown to capture the underlying structure in spherical tumbler flows [9,10] with deviations in experimental models occurring due to the material passing through the flowing layer or diffusivelike effects from particle-particle interaction.

In applications of mixing, whether industrial or natural, it is a primary interest to quantify the rate of mixing to a certain condition. Molecular diffusion acting alone will cause a concentration field to tend to uniformity at an exponential rate, although this rate is generally very slow. Good stirring protocols can increase the rate to uniformity. In fully chaotic flows exponential stretching and compression of a fluid parcels produce an exponential rate in the reduction of length scales and an increase in the material interface. However, Kolmogorov-Arnold-Moser surfaces and islands, boundaries surrounding fully chaotic domains, or parabolic points can contaminate this exponential mixing rate [11,12]. The process of cutting and shuffling increases the number of interfaces linearly [13] and has been proven to be weak mixing in the asymptotic limit even in the absence of material stretching [14], but the mixing rate is at most polynomial [15]. Piecewise isometries on the unit interval or on a hemispherical shell have been shown to achieve good mixing even in finite time [16–18]. However, these mixing processes are unlikely to arise in isolation in real life applications.

There is an extensive literature studying the combination of stretching and folding from chaotic advection and diffusion and the underling mechanisms which drive the mixing rates. Uniform stretching with diffusion predicts an unrealistic

*mm10hek@leeds.ac.uk

superexponential mixing rate, however nonuniformity in the underlying flow field produces exponential mixing rates overall. This rate is governed either through the misalignment of concentration field gradients with local stretching directions [19] or the global transport rate of the underlying flow field [20–23]. The global regime leads to the emergence of "strange eigenmodes" [24], persistent patterns with a fixed exponential decay rate. The decay rate of the dominant eigenmode becomes independent of diffusivity in the zero-diffusivity limit [20,22,24].

Permutations of equally sized cells on the unit interval, a subset of interval exchange transformations (IETs), have been shown to accelerate the asymptotic mixing rate of diffusion acting alone [25]. IETs with diffusion have been used as simple mappings to investigate optimizing diffusion [26] and comparing measures of mixing [27]. Bounds have been found on the mixing rates for permutations composed with expanding maps on the unit interval with the conclusion that permutations do not improve the mixing rate and typically make it worse [28]. It similarly is reported for shears composed with a slip deformation that the combined mechanisms can slow the rate of mixing of material segregation [29].

In this paper we investigate the composition of the three dynamics of SF, CS, and diffusion and the resulting mixing rates. We begin to address this here by studying a simple map on the unit interval of an idealized time-periodic and laminar fluid flow. In Sec. II we construct the problem and introduce the hyperbolic and discontinuous maps. In Sec. III we present the numerical results, and in Sec. IV we discuss the relationships to previously published results on expanding maps with permutations. In Sec. V we consider the results in physical finite time mixing, and the implications of the results are discussed in Sec. VI.

II. FORMULATION OF THE PROBLEM

A. Iterative advection-diffusion map

We study the evolution of a passive scalar $c(\boldsymbol{x},t)$ in a viscous fluid flow by the advection-diffusion equation,

$$\partial_t c(\boldsymbol{x},t) + u(\boldsymbol{x},t)\cdot\nabla c(\boldsymbol{x},t) = \kappa\nabla^2 c(\boldsymbol{x},t), \tag{1}$$

over a domain Ω. The velocity field $u(\boldsymbol{x},t)$ is taken to be incompressible, $\nabla\cdot u = 0$, and time periodic such that $u(\boldsymbol{x},t+T) = u(\boldsymbol{x},t)$. The diffusion coefficient κ is the inverse of the Péclet number $\kappa = \mathrm{Pe}^{-1}$, a nondimensional number representing the ratio of diffusive to advective time scales.

We simplify the evolution of the advection-diffusion equation by separating the processes of advection and diffusion in time. This iterative approach has been used previously to study mixing rates in one- and two-dimensional chaotic maps [20–22]. First we evolve the scalar field according to (1) with $\kappa = 0$ for a time T. Since we are considering laminar time-periodic flows, we consider the advective step as a map $M:\Omega\to\Omega$ acting on fluid particles within the domain Ω as an iterative step in time $t\to t+T$ along the streamlines of the underlying flow field. Then the evolution of $c(\boldsymbol{x},t)\to c(\boldsymbol{x},t+T)$ can be represented by a linear operator acting on the space of functions $P_M:\mathcal{X}\to\mathcal{X}$, $c\in\mathcal{X}$. We consider the function class of piecewise smooth functions on the unit interval $\mathcal{X} = C_p^\infty[0,1)$ as we are interested in studying transformations with discontinuities. The operator for the map is known as the Frobenius-Perron operator in the dynamics literature capturing the evolution of densities.

Following the advective time step, we then include diffusion by evolving the scalar field according to (1) with $u = 0$ via the operator $P_D:\mathcal{X}\to\mathcal{X}$, $P_D = \exp(t\kappa\nabla^2)$ for a time T. The operator for the full advective-diffusive time step then is considered as a composition of the operators $P = P_D\circ P_M$ such that $c^{(j+1)}(x) = (Pc^{(j)})(x)$ with $j = 0,1,2,\ldots$ denoting the discrete steps. The operator P is linear due to the linearity of the advection-diffusion equation (1).

The eigenvalues λ_k of the operator P and their respective eigenfunctions v_k satisfy $Pv_k = \lambda_k v_k$, and the eigenvalues can be ordered according to their absolute values by $|\lambda_1|\geqslant|\lambda_2|\geqslant\cdots\geqslant 0$. The trivial eigenvalue $\lambda_1 = 1$ and the respective invariant eigenfunction is the mean field of the scalar $\bar{c}$. All other eigenvalues will have the value of $|\lambda_k| < 1$ when the diffusion coefficient is nonzero.

We take a one-dimensional concentration field and the domain Ω to be the unit interval $\mathbb{T} = [0,1)$ with periodic boundary conditions. Then the concentration field can be represented by the discrete Fourier expansion,

$$c^{(j)}(x) = \sum_{n=-\infty}^{\infty}\hat{c}_n^{(j)}e^{2\pi inx}.$$

The action of the operator P then is represented by the transfer of amplitude between the Fourier coefficients $\hat{c}_n$, given by

$$\hat{c}_n^{(j+1)} = \sum_{k=-\infty}^{\infty} d_{nm}M_{mk}\hat{c}_k^{(j)}, \tag{2}$$

where the transfer matrix due to the advective map M is

$$M_{mk} = \int_0^1 e^{2\pi imx - 2\pi ikM(x)}dx, \tag{3}$$

and the diffusive step is defined via the transfer matrix,

$$d_{nm} = \delta_{nm}\rho^{n^2}, \quad \rho = \exp(-4\pi^2\kappa T). \tag{4}$$

The time period for the diffusive step is normalized ($T = 1$) so that the effect of diffusion is parametrized by κ only.

B. Maps of interest

The two-dimensional incompressible baker's map is a paradigm example of a hyperbolic chaotic map, which is mixing, given by the map,

$$M_B(x,y) = \begin{cases}(x/2,2y) & \text{for } y\in[0,1/2),\\ ([x+1]/2,2y-1) & \text{for } y\in[1/2,1).\end{cases} \tag{5}$$

By considering a y independent initial condition, the baker's map reduces to a one-dimensional map which is one-to-two and represented acting on the concentration field by

$$c^{(j+1)}(x) = \begin{cases}c^{(j)}(2x) & \text{for } x\in[0,1/2),\\ c^{(j)}(2[x-1]) & \text{for } x\in[1/2,1).\end{cases}$$

Figure 1 depicts the action of the baker's map and its reduction to one dimension.

We compose the baker's map with the simplest nontrivial piecewise isometry on the unit interval, a permutation of

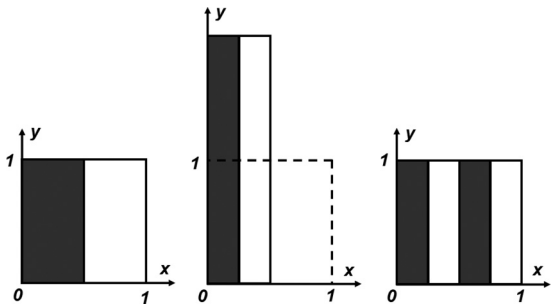

FIG. 1. The action of the baker's map (5) is to contract the x direction, stretch the y direction, and reassemble onto the unit torus. Taking a y independent initial condition, here $c(x,y) =$ gray for $x < 1/2$ and $c(x,y) =$ white for $x \geqslant 1/2$, the baker's map is reduced to a one-dimensional map on the unit interval.

equally sized cells. The permutation map is applied by first dividing the unit interval into N equally sized intervals and numbering them according to their position within the interval. Consider a permutation $\sigma \in S_N$, where S_N is the group of all permutations on the set of symbols $\{1,2,\ldots,N\}$. Then the action of the map on a point $x \in [(l-1)/N, l/N)$ is given by

$$M_\sigma(x) = x + \frac{\sigma(l) - l}{N}. \tag{6}$$

The action on the concentration field is $c^{(j+1)}(x) = c^{(j)}(M_\sigma^{-1}(x))$. The permutations are represented in disjoint cycle notation, see Ref. [25], for example.

The composition of the maps M_B and M_σ will be denoted as a single map $\sigma \circ M_B$. The advantage of the chosen maps is that they are simple to implement in the transfer between Fourier coefficients. The advection-diffusion operator is represented as a single matrix by the product of matrices,

$$\hat{c}_k^{(j+1)} = P_{nk}\hat{c}_n^{(j)}, \quad P_{nk} = d_{nm}M_{mk},$$

where the diffusive step matrix is taken as in (4) and the advective step,

$$M_{mk} = \int_0^1 e^{2\pi i m x - 2\pi i k[\sigma \circ M_B(x)]} dx$$
$$= \frac{(1-\omega^{(2k-m)})}{2\pi i(2k-m)} \sum_{\ell=1}^{N} \omega^{m\sigma(\ell)-2k\ell}$$

when $m \neq 2k$ with the primitive Nth root of unity $\omega = e^{-2\pi i/N}$. When $m = 2k$,

$$M_{mk} = \frac{1}{N} \sum_{\ell=1}^{N} \omega^{m[\sigma(\ell)-\ell]}.$$

The computational process is then to truncate the Fourier modes to deal with finite matrices. Here we take $-K \leqslant k \leqslant K$ with $K = 1000$, which was sufficient for $\kappa \geqslant 10^{-6}$. Larger values of K showed no change in computational results. K can be increased accordingly for smaller values of κ.

We measure the decay of variance from the uniform distribution,

$$\psi(j) = \int_0^1 |c^{(j)}(x) - \bar{c}|^2 dx = \sum_k \left|\hat{c}_k^{(j)}\right|^2, \tag{7}$$

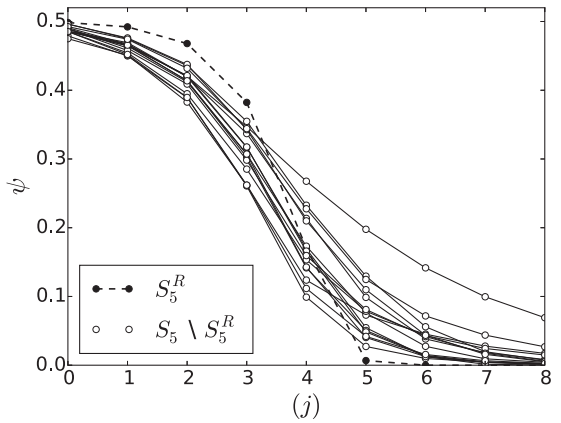

FIG. 2. The initial stages of variance decay for representative permutations. Permutations which introduce new interface $S_5 \backslash S_5^R$ deplete the variance quicker than the identity of rotational permutations S_5^R in the initial three iterations. The diffusion coefficient is $\kappa = 10^{-5}$ with the initial condition $c^{(0)}(x) = \cos(2\pi x)$.

to quantify the mixing rate. Subtracting the mean value $\bar{c}$ as a constant, the rate of decay of variance is calculated in its approach to zero. A map which has good mixing will ensure that $c(x) \to \bar{c}$ quickly.

In the interest of the discussion here we only present results for $\sigma \in S_5$. For ease of discussion we define the rotation subgroup of S_N as the permutations σ which satisfy

$$\sigma(l) = l + m \mod N$$

for $m \in \{0,1,\ldots N-1\}$. Note that we have included the identity permutation in this group, which we denote S_N^R.

III. NUMERICAL RESULTS

A. Initial transient

Figure 2 shows the decay of variance for a selection of permutations with $\kappa = 10^{-5}$ and the initial condition $c^{(0)}(x) = \cos(2\pi x)$. For a permutation $\sigma \in S_5^R$, the map reduces to $M(x) = 2x + m/N \mod 1$. Then $M_{mk} = \omega^{mk}$ for $m = 2k$ with $|\omega^{mk}| = 1$ and $M_{mk} = 0$ when $m \neq 2k$. Hence the resulting variance equation can be calculated analytically for all $\sigma \in S_N^R$, and for the initial condition $\cos(2\pi x)$ we have

$$\psi(j) = \psi(0)\exp\left(-\tfrac{32}{3}\pi^2\kappa(4^j - 1)\right). \tag{8}$$

This result is the same as discussed in Ref. [21]. There is an exponential cascade to large wave numbers where the action of diffusion is more effective, leading to superexponential decay in the variance. This is observed in the linear-log plot in Fig. 3 for a representative permutation (12 345).

For all other permutations $\sigma \in S_5 \backslash S_5^R$ the permutations create additional interfaces, transferring concentrations to large wave numbers in the Fourier expansion immediately. These additional sharp interfaces are not captured by stretching histories which implies that any local Lagrangian arguments will break down in predicting the mixing rate of such a system. However, once there is a significant depletion of variance, the incompressible baker's map composed with $\sigma \in S_5^R$ depletes the variance quicker than any $\sigma \in S_5 \backslash S_5^R$.

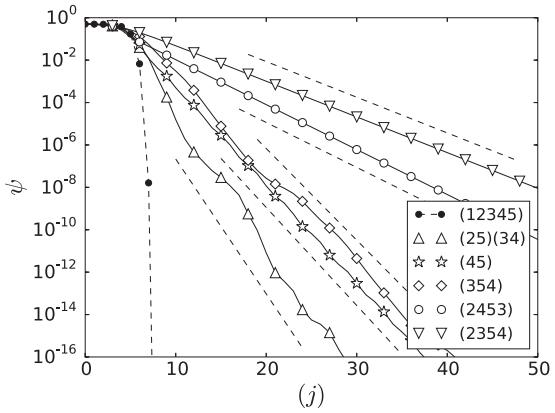

FIG. 3. Variance decay profiles for representative permutations on a linear-log plot. The dashed lines show the variance decay predicted by the second leading eigenvalues λ_2. The diffusion coefficient is $\kappa = 10^{-5}$ with the initial condition $c^{(0)}(x) = \cos(2\pi x)$.

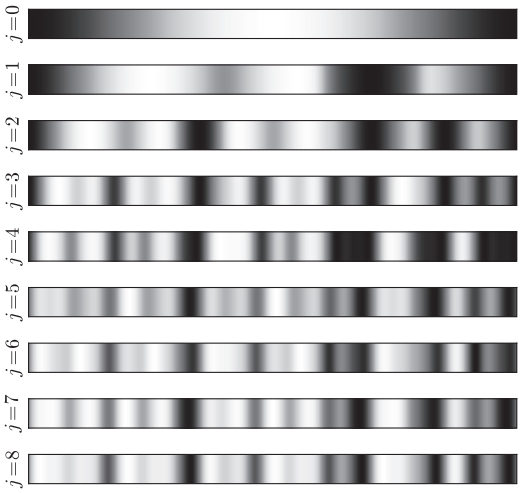

FIG. 4. The image shows the first few iterations for the composed map with $\sigma \circ M_B$ with $\sigma = (34)$, $\kappa = 10^{-4}$ and the initial condition $c^{(0)}(x) = \cos(2\pi x)$. The color scale is adjusted at each iteration to clearly show the persistent pattern emerging.

B. Exponential decay

For all $\sigma \in S_5 \backslash S_5^R$ the decay in concentration variance in the long-time limit is exponential. A sample of the variance profiles is seen in Fig. 3 for the initial condition $c^{(0)}(x) = \cos(2\pi x)$ and $\kappa = 10^{-5}$. The variance profiles show significant variation in the exponential rates of decay for different permutations. Similar variation is also seen across a range of diffusivity coefficients.

The decay rates are predicted from the transfer matrices of the composed advection-diffusion iterative map P_{nk}. After a number of initial iterations the eigenfunctions v_k decay at the rate of their respective eigenvalues until the slowest decaying eigenfunction with the slowest decay rate, which is the second leading eigenvalue λ_2, dominates the evolution of the concentration field. Hence the long-time exponential decay rate of the variance is given by $\psi(j) \sim |\lambda_2|^{2j}$, intuitive from (7). If $|\lambda_2| \sim 1$, then the decay rate of the dominant eigenfunction v_2 would be slow, whereas $|\lambda_2| \ll 1$ predicts a fast mixing rate.

The predicted decay rates from the eigenvalues are plotted as dashed lines in Fig. 3 to show the precise agreement with the respective profiles. Oscillations arise due to the complex value of the eigenvalues and eigenfunctions [30]. The eigenfunctions are either static or spatially evolve on further applications of the operator P_{nk}. Figure 4 shows the emergence of a static eigenfunction for the permutation $\sigma = (34)$ after a number of initial iterations. Randomizing the amplitudes of the first four modes for the initial condition [30] results in the same eventual exponential decay rate. Hence we conclude that these are persistent patterns with decay rates irrespective of the initial condition, similar to those seen in chaotic advective systems with nonuniformity in the stretching rates of the flow field.

This is the well known global mechanism for mixing in smoothly deforming systems [20–22]. Dispersion between the Fourier modes occurs due to the permutation composition, comparable to the dispersion in nonuniform maps [21]. The decay rate is not governed by the local Lagrangian behavior since the stretching rates are the same almost everywhere except for a countable number of discontinuities which form a set of zero measure. Nonuniformity arises in the rearrangement of striations by the interval exchange. Diffusive and reactive systems have been shown previously to be sensitive to striation arrangement [31]. However, unlike the strange eigenmodes of nonuniform smooth systems which align with regions of low stretching, the eigenmodes do not appear to correlate with physical characteristics of the underlying advective dynamics, such as periodic points or where the discontinuities are introduced.

According to the second leading eigenvalues $|\lambda_2|$ for different diffusivity rates each permutation falls into one of 16 subgroups of S_5. The subgroups consist of five or ten permutations with $|\lambda_2|$ the same for all values of κ. The subgroups reflect rotations and reflections in the dynamics of the compositions on $\mathbb{T} = [0,1)$ which is not intuitive from the permutations alone. For the rest of the paper we ignore $\sigma \in S_5^R$ and focus on permutations which have long-time exponential decay of variance.

C. Effect of κ

A representative permutation from each of the 15 remaining subgroups was chosen, and the second leading eigenvalues were computed for many values of κ. Figure 5 shows several of the profiles which highlight the behavior seen. For some of the permutations there is convergence in the limit of $\kappa \to 0$, and the approach is monotonic with the diffusion coefficient, for example, (2453) and (45). Convergence of mixing rates in the limit of small diffusivity is well observed numerically in nonuniform smooth chaotic deformations [20,24,32].

However nonmonotonic profiles of the decay rates also occur with changing κ, for example, (24), (354), and (2354), which have not been widely reported. If the subgroups were listed by the value of $|\lambda_2|$, then it is apparent from Fig. 5 that the ordering would be dependent on the value of κ. Reference [25] observed similar behavior for permutations composed with diffusion, however nonmonotonicity was not reported. Examples of maps in which nonmonotonicity has been seen include an expanding map with three branches [33]

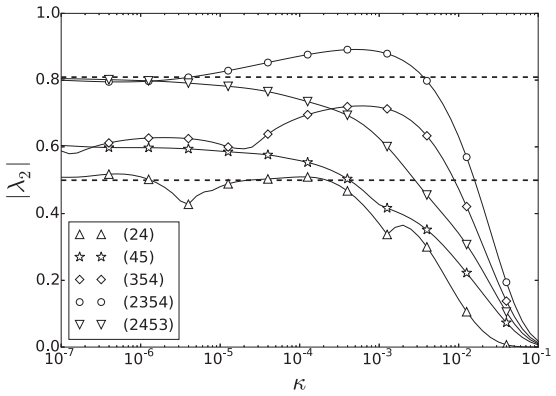

FIG. 5. $|\lambda_2|$ is plotted against κ for a number of permutations. Convergence in the limit $\kappa \to 0$ occurs for some of the permutations, whereas $|\lambda_2|$ changed nonmonotonically for others. The dashed lines represent theoretical upper and lower bounds in the limit $\kappa = 0$. The symbols are used to distinguish the profiles and do not represent data points.

and the nonuniform inverted baker's map with a no-flux boundary condition where a power law relation had oscillatory nonmonotonic behavior [34]. Both maps contain points that are nondifferentiable.

IV. MIXING RATES IN THE NONDIFFUSIVE LIMIT

In the absence of diffusion the variance of the concentration field would remain constant, however the advective operator P_M can be said to be mixing in the following sense [35]. Take sets $A, B \subset \Omega = [0,1)$ and define the Lebesgue measure μ such that $A = [a,b)$ so that $\mu(A) = b - a$. Let $(\Omega, \mathcal{A}, \mu)$ be a normalized measure space where $\mathcal{A}$ is the σ algebra made up of all possible half-open subsets of the unit interval and $M: \Omega \to \Omega$ is a measure-preserving transformation. Then M is said to be *mixing* if

$$\lim_{n\to\infty} \mu(A \cap M^n(B)) = \mu(B)\mu(A) \text{ for all } A, B \subset \mathcal{A}. \quad (9)$$

For a map M which is not invertible we replace M^n with M^{-n}. This states that, under the action of the map on the set A, we expect to find the same amount of A in any of the chosen intervals B. This can be reformulated in functional form as the action of the map M on observable functions g and h via the *decay of correlations*,

$$C_{g,h}(n) = \left| \int h(g \circ M^{-n}) d\mu - \int g \, d\mu \int h \, d\mu \right|. \quad (10)$$

The rate at which $C_{g,h}(n) \to 0$ is of interest. Typically the observables g and h are representative of a scalar field. We refer to the following lemma from Ref. [36]:

Lemma 1. For the Frobenius-Perron operator P which represents the map M, let $\mathcal{X}$ be a class of real-valued functions preserved by P. Let $\sigma(P)$ denote the spectrum of P when considered as an operator on $\mathcal{X}$, and set $\tau = \sup\{|z|: \in \sigma(P)\backslash\{1\}\}$. Then there is a constant $C < \infty$ such that $C_{gh}(N) \leqslant C\tau^N$ for all $N \geqslant 0$ if $g \in L^\infty$ and $h \in \mathcal{X}$.

Hence the decay of correlations and thus the rate of mixing τ is bounded by the second leading eigenvalue of the spectrum of P. It previously has been shown that the mixing rate given by the second leading eigenvalue in the small diffusivity limit tends to the second leading eigenvalue of the isolated spectrum for the advective operator P_M in smoothly deforming systems [32].

Thus, studying the spectrum of P_M will give an insight into the mixing rate of the composed map as $\kappa \to 0$. However, for $\kappa = 0$ the transfer matrix for the Fourier coefficients can not be truncated feasibly, thus it cannot be found from the computational method already presented. The rate of mixing for the map when $\kappa = 0$ can be calculated from matrices defining the probability transition between Markov partitions for the map, the derivation of which closely follows methods developed for permutations composed with expanding maps, and we briefly outline the results of Ref. [28].

An expanding map on the unit torus $[0,1)$ is described as

$$f(x) = mx \mod 1, \quad m \in \mathbb{Z}, \quad m \geqslant 2, \quad (11)$$

and the composition of expanding maps and permutations is denoted $\sigma \circ f$. The eigenvalues of Markov transition matrices representing the composed maps are related to the isolated spectrum of the composed map $\sigma \circ f$ through the use of Fredholm matrices. The absolute value of the second leading eigenvalue for the transition matrix is the value τ. It is proved that whenever N is not a multiple of m, the composition $\sigma \circ f$ acting on functions of bounded variation is always mixing, that is, $\tau < 1$. A lower bound on τ is found to be $1/m$, and when $N > m$ and $gcd(m,N) = 1$,

$$\tau \leqslant \tau_{\max} = \frac{\sin(m\pi/N)}{m \sin(\pi/N)} \quad (12)$$

is a suitable upper bound.

The construction and results of Ref. [28] have a direct comparison with the current presented model. Consider the graphical representation of the system studied here; the halving map composed with a permutation, shown in Fig. 6. We denote the preimage $(\sigma \circ M_B)^{-1}$, which also is presented graphically. It is possible to construct a Markov partition on the preimage map with $2 \times N$ elements of equal size $1/2N$ (N is the number of cells in the permutation). It can easily be shown that an eigenvalue τ of the transformation $\sigma^{-1} \circ f$ is equivalent to the eigenvalue τ of $(\sigma \circ M_B)^{-1}$, where σ^{-1} denotes the inverse permutation of σ. This arises from the construction of the Markov transition matrices in the proof of the bounds from Ref. [28] (see the Appendix for details).

In reference to the definition of mixing given in (9), $(\sigma \circ M_B)^{-1}$ is not invertible, and as such, action of the map $\sigma \circ M_B$ is considered, which is precisely the evolution of striations we have studied here. Thus we compare the rates of mixing in the limit $\kappa \to 0$ to those predicted from the Markov transition matrices of $(\sigma \circ M_B)^{-1}$.

Table I compares τ for the preimage $(\sigma \circ M_B)^{-1}$ with $|\lambda_2|$ of the respective diffusive transfer matrices in the limit of small diffusivity. The values show good agreement for many of the permutations, however this is not the case for all. Considering the permutations which are not in good agreement, profiles of $|\lambda_2|$ with κ for these permutations have nonmonotonic behavior with significant variation in the values of $|\lambda_2|$. It is not known whether the profiles eventually will converge or continue oscillating in the limit of small diffusivity, but investigating smaller values of κ is computationally infeasible.

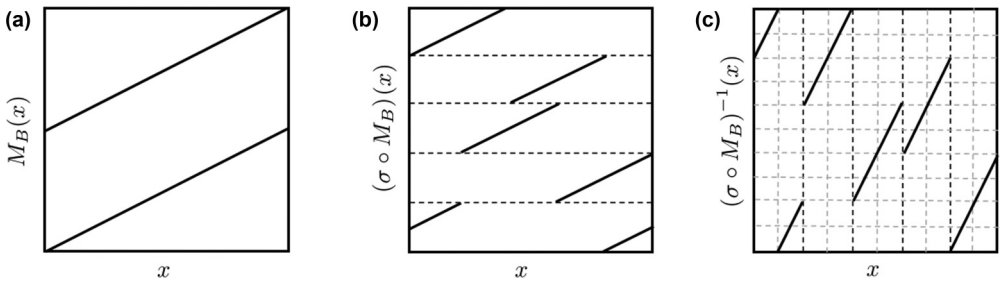

FIG. 6. Graphical representations of (a) a one-dimensional approximation of the baker's map, the halving map, (b) the halving map composed with the permutation $\sigma = (15\,243)$, denoted $(\sigma \circ M_B)$, and (c) the preimage map $(\sigma \circ M_B)^{-1}$ is shown with an appropriate Markov partition.

The lower and upper bounds, respectively, on the value of τ for the model considered here are

$$\tau_{\min} = \frac{1}{2}, \qquad \tau_{\max} = \frac{\sin(2\pi/5)}{2\,\sin(\pi/5)} \approx 0.809,$$

and are plotted as dashed lines in Fig. 5. $\tau_{\max}$ and $\tau_{\min}$ predict the slowest and fastest mixing rates, respectively, of the operator $P_{\sigma\circ M_B}$ for $\sigma \in S_5$ and seem to be reasonable bounds on the mixing rate when the diffusive rate is small. However, at large values of κ the upper bound does not agree as a bound on $|\lambda_2|$ due to the nonmonotonicity of the profiles. For many of the permutations in the composed maps the second leading eigenvalue τ given by the Markov transition matrix is smaller than $|\lambda_2|$ for nonzero κ. Counterintuitively this implies that the mixing rate is slower when the diffusive effect is large compared to the diffusivity in the zero limit.

Explaining the nonmonotonicity is beyond the scope of this paper, although nonmonotonicity in profiles of mixing rates with κ appear to persist when other hyperbolic maps on the unit interval are considered for the stretch and fold component, such as when the baker's map is the incompressible nonuniform baker's map [20] or inverted baker's map [34,37]. The computational results of these maps composed with permutations are omitted for brevity.

V. FINITE TIME MIXING

The results of the paper thus far have been concerned with asymptotic mixing rates of the composed maps. However, mixing of concentration fields has several stages which contribute to the finite time mixing and in practical situations one would want to consider the time needed to mix to a desired condition. We consider the finite mixing rate by first returning to means of quantifying mixing under the action of advection and diffusion. We introduce the L^∞ and L^q norms,

$$\begin{aligned} L_t^\infty &= \|c(x,t) - \bar{c}\|_\infty \\ &= \inf\{M : |c(x,t) - \bar{c}| \leqslant M \text{ a.e. } x \in [0,1)\}, \end{aligned}$$

and

$$L_t^q = \|c(x,t) - \bar{c}\|_q = \left(\int_0^1 |c(x,t) - \bar{c}|^q dx\right)^{1/q}.$$

In this paper we already have considered the variance which is defined as $\|c(x,t) - \bar{c}\|_2^2$, the square of the L^2 norm. Which norm to consider depends on the application and desired result. Note that for $0 < q' \leqslant q$ then $\|\cdot\|_q \leqslant \|\cdot\|_{q'} \leqslant \|\cdot\|_\infty$. Similar to a previous study [25], we consider the time needed for a desired norm to come within an arbitrary condition, say 5% of uniform, which is referred to as the *time to 95% mixing* t_{95}. It is defined to be the smallest $t_{95} = t > 0$ such that

$$\|c(x,t) - \bar{c}\|_q / \|c(x,0) - \bar{c}\|_q \leqslant 0.05, \tag{13}$$

where q denotes the L^q norm. We numerically investigate the number of iterates needed to satisfy this requirement for the L^∞ norm and ψ.

In the initial stages of advection and diffusion, when the effect of diffusivity is small, an L^q norm will remain constant for some time until the gradients or length scales in the concentration field are on the order of the Batchelor length scale $\sqrt{\kappa/\lambda_{\text{ls}}}$, the balance between diffusive rate and local strain rate λ_{ls}. For smoothly deforming chaotic flows, in the limit of small diffusivity the exponential mixing rate becomes independent of the diffusivity coefficient in the limit of small diffusivity, thus the main consequence of decreasing the effect

TABLE I. For each of the subgroups, the absolute value of the second leading eigenvalues for low values of the diffusion coefficient, denoted $|\lambda_2^\kappa|$, are computed. A comparison with τ, the mixing rate from the respective Markov transition matrices of the preimage mapping $(\sigma \circ M_B)^{-1}$, shows good agreement.

	(45)	(34)	(345)	(354)	(35)	(23)(45)	(2354)	(2453)
$\lvert\lambda_2^{10^{-7}}\rvert$	0.6042	0.6444	0.673	0.5878	0.6013	0.7493	0.7996	0.8046
$\lvert\lambda_2^{10^{-8}}\rvert$	0.6061	0.6518	0.6641	0.6235	0.5904	0.753	0.8075	0.807
Markov τ	0.5919	0.6624	0.6677	0.5755	0.5755	0.7564	0.809	0.809
	(24)	(245)	(253)	(25)	(25)(34)	(13452)	(1345)	
$\lvert\lambda_2^{10^{-7}}\rvert$	0.5751	0.8048	0.6443	0.6086	0.5089	0.8075	0.6156	
$\lvert\lambda_2^{10^{-8}}\rvert$	0.561	0.8072	0.6531	0.5926	0.4788	0.807	0.5808	
Markov τ	0.5	0.809	0.6624	0.5919	0.5	0.809	0.5	

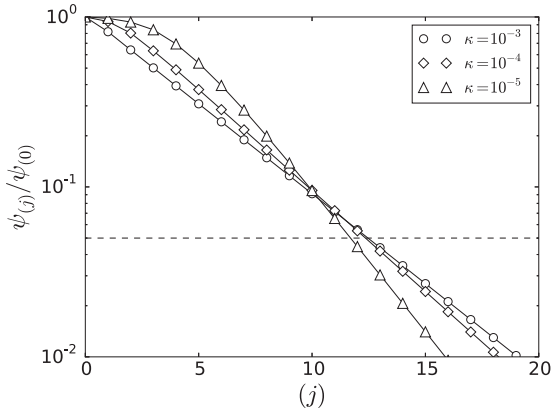

FIG. 7. The variance $\psi(j)/\psi(0)$ is plotted for $\sigma \circ M_B$ with $\sigma = (2354)$, initial condition $c^{(0)}(x) = \cos(2\pi x)$ for three diffusivity values. The linear-log plot is used to better distinguish the iterates in which $\psi(j)/\psi(0)$ crosses the 95% threshold, represented by the the dashed line. $\psi(j)/\psi(0)$ crosses the threshold at the earliest time when $\kappa = 10^{-5}$, the smallest value.

of diffusivity is to extend the initial transient where a measured norm is close to constant. Once the Batchelor scale is reached there is significant decay, however this initial stage is weakly dependent on diffusivity, on the order of $\log(\kappa)$ [21,38].

As an example, we take the permutation $\sigma = (2354)$, which has a slower asymptotic mixing rate at nonzero κ than the upper bound on the zero-diffusivity mixing rate. The initial condition is taken to be $\cos(2\pi x)$. Figure 7 plots the variance decay rates for three different values of κ. The renormalized variance of $c^{(j)}(x)$ for the larger values of $\kappa = 10^{-3}, 10^{-4}$ achieves the 95% mixed state after the smallest value of $\kappa = 10^{-5}$, although the difference is approximately one iteration. However, for the L^∞ norm in Fig. 8, the condition for the larger diffusivity rates is reached approximately five iterations later. This example illustrates that the counterintuitive deceleration with diffusivity rate κ could have a significant effect on the time to achieve a practical mixing condition. In applications of fluid mixing devices this would equate to five additional stirring periods or channel segments to achieve the desired result, which could be overlooked if approximating mixing time from advective properties only and thus the correct mixing criteria not achieved in the predicted time.

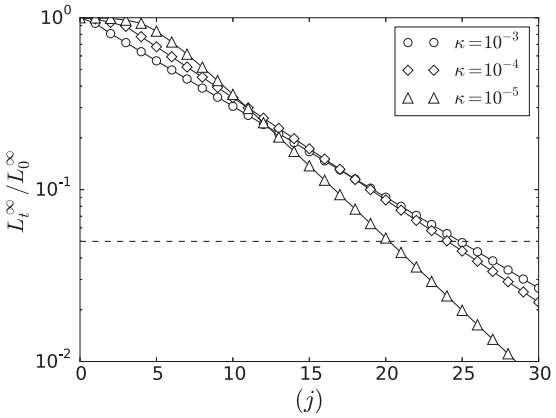

FIG. 8. The L_t^∞/L_0^∞ norm is plotted for $\sigma \circ M_B$ with $\sigma = (2354)$, initial condition $c^{(0)}(x) = \cos(2\pi x)$ for three diffusivity values. The linear-log plot is used to better distinguish the iterates in which L_t^∞/L_0^∞ crosses the 95% threshold, represented by the dashed line. Similar to the variance, L_t^∞/L_0^∞ crosses the threshold at the earliest time when $\kappa = 10^{-5}$, the smallest value.

VI. DISCUSSION

We have presented a one-dimensional model which captures a mixture of stretching and discontinuous advective dynamics with a diffusive step. In the initial transient the additional discontinuities speed up the decay of variance over the chaotic advection alone. However once the Batchelor scale is reached and variance begins to deplete, a phase of exponential decay begins due to the nonuniformity caused by the permutation of the striation arrangement. Lagrangian arguments fail to explain the varying decay rates across the range of permutations since stretching rates are the same almost everywhere except where they are undefined on the discontinuities which form a set of measure zero. The mechanism for the emergence of an exponential asymptotic mixing rate is global, and in the limit $\kappa \to 0$ the mixing rate is well approximated by the global transport rate predicted from the Markov partitions of the preimage map.

However, this approach to the mixing rate in the zero-diffusivity limit is nonmonotonic in many cases, which is counterintuitive. Although nonmonotonicity has been observed in one-dimensional maps before [34] [33], here a slower mixing rate than the global mixing rate is predicted for large values of the diffusivity coefficient. However, all maps in which nonmonotonicity with diffusion has been reported have a common property in that they contain points which are nondifferentiable. We hypothesize that this deceleration with diffusion is a feature of noncontinuous mappings in which discontinuous transformations are a subset. In the dynamical systems and ergodic theory literature there is great interest in finding global mixing rates of advective maps and bounds on these mixing rates, but these computational results suggest that, in studying fluid mixing systems in which there is a mixture of stretching and cutting and shuffling, diffusion may have to be taken into account for accurate mixing rate predictions and comparisons across mixing protocols. The significance in this observation is shown to effect mixing rates in finite time considerations to achieve physical mixing conditions, chosen arbitrarily here to be a 95% mixed state.

The present paper could be extended to a larger collection of interval exchange transformations with finite order, however the similarities of the mixing rates for small diffusivity to the rates τ when $\kappa = 0$ implies that the conclusions of Ref. [28] predict well the asymptotic mixing rates and it is unlikely that adding diffusion would highlight anything of further interest than already discussed herein. The model is idealized highly in relation to real fluid mixing problems. The one-dimensional reduction of the baker's map leads to striation arrangements which are all perfectly aligned with the stable manifolds and, notably, the discontinuities also are aligned with the stable manifolds. One possible extension would be to study the same mixing mechanisms in a two-dimensional system where one of these idealizations is not present.

ACKNOWLEDGMENTS

H.K. would like to thank J.-L. Thiffeault for helpful discussions while visiting the University of Madison-Wisconsin, USA. H.K. was funded by EPSRC via Grant No. EP/L01615X/1.

APPENDIX

In this Appendix we briefly discuss the construction of the Markov partitions and highlight the required results of Ref. [28] to find the mixing rates for $\sigma \circ M_B$ when $\kappa = 0$.

The Markov partitions for the composition map $\sigma \circ f$, where $\sigma \in S_N$ and f as defined in (11), are constructed as follows. Define P_k by $\{0,1,\ldots,k-1\}$, and number the associated rows and columns in the transition matrices from 0. $A(m,N)$ and $B(m,N)$ are defined to be the state transition matrices for the expanding map f with respect to P_N and P_{Nm}, respectively, and are found via

$$A(m,N)_{ij} = \begin{cases} 1, & \text{if } j = mi+d \mod N, \quad 0 \leqslant d \leqslant m-1, \\ 0, & \text{otherwise,} \end{cases}$$

and

$$B(m,N)_{ij} = \begin{cases} 1, & \text{if } j = mi+d \mod Nm, \quad 0 \leqslant d \leqslant m-1, \\ 0, & \text{otherwise.} \end{cases}$$

The state transition matrices for $\sigma \circ f$ then are obtained by permuting the columns of $A(m,N)$ and $B(m,N)$. $P(\sigma)$ is defined as

$$P(\sigma) = \begin{cases} 1, & \text{if } j = \sigma(i), \\ 0, & \text{otherwise,} \end{cases}$$

and let $Q(\sigma)$ be the $Nm \times Nm$ matrix obtained by replacing each entry 1 in $P(\sigma)$ by an $m \times m$ identity matrix and each 0 entry by a $m \times m$ zero matrix. Then the state transition matrices for $\sigma \circ f$ with respect to P_N and P_{Nm} are $A(m,N)P(\sigma)$ and $B(m,N)Q(\sigma)$. It is proved in Lemma 4.2.1 of Ref. [28] that the eigenvalues of $A(m,N)P(\sigma)$ and $B(m,N)Q(\sigma)$ are the same.

When considering the state transition matrices of the preimage $(\sigma \circ M_B)^{-1}$, the same construction can be followed in which the rows are permuted instead of the columns; $P(\sigma)A(m,N)$ and $Q(\sigma)B(m,N)$. By the same arguments in Lemma 4.2.1 [28], a vector space can be constructed which proves that the second leading eigenvalues of $P(\sigma)A(m,N)$ and $Q(\sigma)B(m,N)$ also are equivalent.

Finally, note that $P(\sigma)A(m,N)$ is the matrix obtained from $A(m,N)P(\sigma^{-1})$ and, if $\tilde{\tau}$ is an eigenvalue of $P(\sigma)A(m,N)$, then $\tau = \tilde{\tau}/m$, hence for every σ, $\tau_{\sigma^{-1}\circ f} = \tau_{(\sigma \circ M_B)^{-1}}$.

[1] H. Aref, J. Fluid Mech. **143**, 1 (1984).
[2] J. M. Ottino, *The Kinematics of Mixing: Stretching, Chaos, and Transport* (Cambridge University Press, Cambridge, England, 1989).
[3] D. Hobbs and F. Muzzio, Chem. Eng. J. **67**, 153 (1997).
[4] S. W. Jones and H. Aref, Phys. Fluids **31**, 469 (1988).
[5] J.-M. Hertzsch, R. Sturman, and S. Wiggins, Small **3**, 202 (2007).
[6] D. R. Lester, G. Metcalfe, M. G. Trefry, A. Ord, B. Hobbs, and M. Rudman, Phys. Rev. E **80**, 036208 (2009).
[7] L. D. Smith, M. Rudman, D. R. Lester, and G. Metcalfe, Chaos **26**, 023113 (2016).
[8] D. V. Louzguine-Luzgin, L. V. Louzguina-Luzgina, and A. Y. Churyumov, Metals **3**, 1 (2012).
[9] R. Sturman, S. Meier, J. Ottino, and S. Wiggins, J. Fluid Mech. **602**, 129 (2008).
[10] G. Juarez, I. C. Christov, J. M. Ottino, and R. M. Lueptow, Chem. Eng. Sci. **73**, 195 (2012).
[11] E. Gouillart, O. Dauchot, B. Dubrulle, S. Roux, and J.-L. Thiffeault, Phys. Rev. E **78**, 026211 (2008).
[12] J. Springham and R. Sturman, Ergodic Theory Dyn. Syst. **34**, 1724 (2014).
[13] C. F. Novak, J. Mod. Dyn. **3**, 379 (2009).
[14] A. Avila and G. Forni, Ann. Math. **165**, 637 (2007).
[15] A. Katok, Israel J. Math. **35**, 301 (1980).
[16] M. K. Krotter, I. C. Christov, J. M. Ottino, and R. M. Lueptow, Int. J. Bifurc. Chaos **22**, 1230041 (2012).
[17] M. Yu, P. B. Umbanhowar, J. M. Ottino, and R. M. Lueptow, Int. J. Bifurc. Chaos **26**, 1630038 (2016).
[18] P. P. Park, P. B. Umbanhowar, J. M. Ottino, and R. M. Lueptow, Chaos **26**, 073115 (2016).
[19] T. M. Antonsen, Jr., Z. Fan, E. Ott, and E. Garcia-Lopez, Phys. Fluids **8**, 3094 (1996).
[20] D. R. Fereday, P. H. Haynes, A. Wonhas, and J. C. Vassilicos, Phys. Rev. E **65**, 035301 (2002).
[21] A. Wonhas and J. C. Vassilicos, Phys. Rev. E **66**, 051205 (2002).
[22] J.-L. Thiffeault and S. Childress, Chaos **13**, 502 (2003).
[23] A. Pikovsky and O. Popovych, Europhys. Lett. **61**, 625 (2003).
[24] R. Pierrehumbert, Chaos Solitons Fractals **4**, 1091 (1994).
[25] P. Ashwin, M. Nicol, and N. Kirkby, Physica A **310**, 347 (2002).
[26] G. Froyland, C. González-Tokman, and T. M. Watson, SIAM Rev. **58**, 494 (2016).
[27] R. Sturman, Adv. Appl. Mech. **45**, 51 (2012).
[28] N. Byott, M. Holland, and Y. Zhang, Discrete Contin. Dyn. Syst. **33**, 3365 (2013).
[29] L. D. Smith, M. Rudman, D. R. Lester, and G. Metcalfe, Phys. Rev. E **95**, 022213 (2017).
[30] V. Toussaint, P. Carrière, and F. Raynal, Phys. Fluids **7**, 2587 (1995).
[31] M. Clifford, S. Cox, and E. Roberts, Physica A **262**, 294 (1999).
[32] P. Haynes and J. Vanneste, Phys. Fluids **17**, 097103 (2005).
[33] B. Eckhardt, E. Hascoët, and W. Braun, in *IUTAM Symposium on Nonlinear Stochastic Dynamics* (Springer, Dordrecht, 2003), pp. 415–424.
[34] A. D. Gilbert, Dynam. Syst. **21**, 25 (2006).
[35] R. Sturman, J. M. Ottino, and S. Wiggins, *The Mathematical Foundations of Mixing: The Linked Twist Map as a Paradigm in Applications: Micro to Macro, Fluids to Solids* (Cambridge University Press, Cambridge, England, 2006).
[36] G. Froyland, in *Nonlinear Dynamics and Statistics*, edited by A. I. Mess (Birkhäuser Verlag AG, Berlin, 2001), p. 281.
[37] E. Gouillart, N. Kuncio, O. Dauchot, B. Dubrulle, S. Roux, and J.-L. Thiffeault, Phys. Rev. Lett. **99**, 114501 (2007).
[38] J.-L. Thiffeault, *Transport and Mixing in Geophysical Flows* (Springer, Berlin, 2008), pp. 3–36.